A 2.4 GHz LoRa-Based Protocol for Communication and Energy Harvesting on Industry Machines

A 2.4 GHz LoRa-Based Protocol for Communication and Energy Harvesting on Industry Machines

Giampaolo Cuozzo, Chiara Buratti, Roberto Verdone

***Abstract*—The fourth industrial revolution is paving the way for Industrial Internet of Things applications where large number of wireless nodes, equipped with sensors and actuators, monitor the production cycle of industrial goods. This paper proposes and analyses LoRaIN, a network architecture and MAC-layer protocol thought for on-demand monitoring of industrial machines. Our proprietary system is an energy-efficient, reliable and scalable solution, where the protocol is built on top of LoRa at 2.4 GHz. Indeed, the low-power characteristics of LoRa allow to reduce energy consumption, while Wireless Power Transfer is used to recharge batteries, avoiding periodic battery replacement. High reliability is obtained through the joint use of Frequency and Time Division Multiple Access. A dynamic LoRaIN scheduler manages the communication and recharging phases depending on the tasks assigned to the nodes, as well as the number of monitoring devices. Performance is measured in terms of network throughput, energy consumption and latency. Results demonstrate that the proposed solution is suitable for monitoring applications of industry machines.**

***Index Terms*—Energy Harvesting, IIoT, LoRa, Smart Manufacturing**

I. Introduction

Smart manufacturing is one of the most relevant sectors of application for the Internet of Things (IoT) [1], [2], [3], [4]. Embedding massive amount of sensors and actuators in the control loop of industry machines, can significantly increase productivity and work safety [5], [6]. Nevertheless, such potential is still limited by the use of wired communication technologies; cables constitute an undesired constraint, especially in the presence of moving components. Wireless connectivity can offer much higher degrees of freedom [7]. The 5th Generation (5G) of mobile networks, with its future releases, is expected to fulfill m any o f t he r equirements set by the control loop of industry machines: latency smaller than 1 ms, very high throughput and reliability [8], [9], [10]. However, 5G will imply high costs, and the technology will become available only in some years.

In the meanwhile, many industry players are setting up pilot projects using existing wireless technologies, like Wi-Fi or Bluetooth. They can offer limited performance levels that do not fulfill the requirements of control loops; on the other hand, they can support simpler monitoring applications, with small investments [11], [12], [13], [14]. Industrial solutions already exist based on Wi-Fi[1] or Bluetooth[2]. Unfortunately, both technologies have constraints in terms of energy consumption and the number of sensors/actuators (hereafter denoted as *tags* or *nodes*) that can be mounted on a machine. This is a major issue, because the advantages of smart manufacturing increase as long as tags are low cost, energy efficient, and their density can be large. An interesting alternative is LoRa, with its version working in the Industrial Scientific and Medical (ISM) band at 2.4 GHz [15]. Despite LoRa is a long-range technology, it can be exploited to cope with the huge path losses that characterize typical intra-machine communications, as demonstrated by the measurement campaign that we have carried out, reported in Appendix A. In addition, the low-power feature of LoRa is particularly suited for resource and energy-constrained devices, [16], [17], [18], and its version at 2.4 GHz offers higher data rates and a wider channel availability than the 868 MHz counterpart.

To minimise the size of tags, and avoid frequent battery replacement, Energy Harvesting (EH) is a very attractive technology; on industry machines tags can be recharged either by means of kinetics [19], [20] or through Wireless Power Transfer (WPT); in the latter case, electromagnetic transmitters (called illuminators) have to be deployed on the machine [21], [22]. In this paper, we propose and analyse the performance of LoRaIN (LoRa for INdustrial networks), a novel communication protocol, where nodes communicate using LoRa at 2.4 GHz at the physical layer, a proprietary protocol at the medium access control (MAC) layer, and are recharged via WPT. Therefore, the paper jointly accounts for communication and WPT, by proposing a balance between transmission and recharging needs. High reliability is achieved by combining Time Division (TDMA) and Frequency Division Multiple Access (FDMA), in the context of a hierarchical network architecture, suitably designed for industry machines. The LoRaIN system and protocol have been designed, tested and validated in a real-world context of an industrial project (committed by a large company in the automation machine field to the University of Bologna), which ended-up with a Proof-of-Concept (PoC). Despite the system has met the customer requirements, the PoC has been done with a very limited number of tags, such that the related experimental results are

[1]See https://www.cambiumnetworks.com/solutions/industrial-broadband-solutions/

not suitable to demonstrate the scalability of the proposed solution. To this end, this paper reports some experimental results performed to characterize the harsh environment of an industrial machine and provided as input to a proprietary network simulator implementing the proposed protocol. The network simulator takes as input parameters some realistic values of the hardware used in the PoC, and provides different network-level performance metrics. In addition, some experimental measurements to test the robustness of the system with respect to Wi-Fi interference have been performed.

The remainder of the paper is organized as follows: Section II highlights the position of LoRaIN with respect to the state of the art, Section III describes the reference scenario, the TDMA-FDMA approach and the passage between real-world and simulation. The protocol is then presented in Section IV. Energy consumption, network throughput and application latencies are derived in Section V. Finally, we discuss simulation results and we draw conclusions.

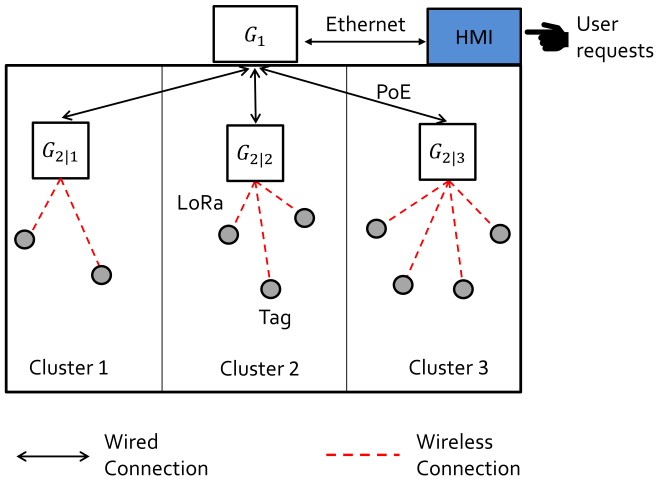

Fig. 1. The LoRaIN network architecture.

II. Related Works

LoRa is the PHY layer technology supporting the development of LoRaWAN, one of the most successful Low Power Wide Area Network (LPWAN) solutions for the IoT.

LoRaWAN uses the 868 MHz ISM band and it is mainly used in outdoor applications, even though some works, such as [23], study its applicability in industrial short-range scenarios. LoRaWAN implements an ALOHA-like communication protocol, widely analysed in the literature (see, e.g, [24], [25], [26], [27], [28]); its performance is therefore affected by the presence of collisions. To overcome this, most approaches rely on TDMA: the Authors of [29] have proposed an improvement based on a centralized TDMA approach; [30] considers a time slotted protocol; [31] shows a solution based on periodic beacons sent by a gateway to ensure network synchronisation; an indoor office test-bed is presented in [32], where a cluster-based architecture utilizes a centralized TDMA approach. In summary, TDMA with centralised scheduling, such as clusterized architectures have been already proposed for improving performance of LoRaWAN networks, however, there is no paper dealing with a time division approach based on LoRa at 2.4 GHz, which offers larger bands and throughput, with respect to the version at 868 MHz. Indeed, the scientific literature is only opening now to this version of LoRa, with studies on its coverage [33] and ranging capabilities [34], as well as on the interference coming from other systems, like Wi-Fi [15] or Long Term Evolution [35]. The coexistence of LoRa and Zigbee in the 2.4 GHz band is further investigated in [36], where the Authors propose a message exchange among these two technologies to optimize the performance of a mesh network.

As far as energy management is concerned, EH in industrial applications can be achieved in different ways [37], [38], [39], [40], [41]; we focus here on WPT, owing to its flexibility. In [42] a magnetically coupled resonance WPT for LPWAN applications has been tested. However, such work does not consider the interference effect between WPT and data communication. On the contrary, we propose a TDMA protocol, which alternates between WPT and communication phases, adapting them to the tasks pursued by the tags on the machine; the LoRaIN scheduler manages the duration of the two phases.

In conclusion, to the best of our knowledge, no existing works have analysed LoRa at 2.4 GHz within an industrial scenario and, in particular, no studies include time-division protocols which use this technology in conjunction with a WPT technique.

III. System Model

A. Reference Scenario

The reference scenario and application refer to the monitoring of an industrial machine. To this aim, tags equipped with different type of sensors (e.g., accelerometer, temperature, humidity, etc.) are deployed in the different parts of the machine and they have to send the measured data upon explicit request from the human operator. To this aim, each machine is equipped with a HMI (Human to Machine Interface), having the role of recognizing the operator request, forwarding them to the LoRaIN system, waiting for replies and displaying the measured parameters. The LoRaIN system is composed of a First-Level Gateway, hereafter denoted as G_1, connected via Ethernet to the HMI and forwarding data via Power over Ethernet (PoE), to one or more Second-Level Gateway(s), hereafter denoted as $G_{2|i}$. The latter are communicating wirelessly with the tags deployed on the machine, using the LoRaIN proprietary protocol. The following subsection will describe in more details the LoRaIN architecture.

B. The LoRaIN Architecture

The LoRaIN network architecture is shown in Figure 1.

The HMI, receiving commands from the operator, is connected via Ethernet to G_1.

The network is partitioned into sub-networks, denoted as clusters. Industrial machines are typically formed by different portions, called sections, which are physically separated by metal slabs, and therefore they are almost electromagnetically isolated. A cluster may coincide to a section, or the latter

may be subdivided into a limited number of clusters; in this paper, for the sake of simplicity, it is assumed that a section corresponds to a cluster. Each cluster is managed by a Second-Level Gateway, $G_{2|i}$, connected via Power over Ethernet (PoE) to G_1. On the other hand, each $G_{2|i}$ is wirelessly connected to the tags of its cluster using LoRa at 2.4 GHz at the physical layer and LoRaIN at the upper layer.

As far as the radio modules are concerned, tags have a single LoRa radio transceiver (the SX1280 [43]), while each $G_{2|i}$ is equipped with three radio transceivers: two are used for exchanging messages with tags, and the other for WPT. We will refer to the functionality of $G_{2|i}$ intended as source of electromagnetic energy for WPT, as illuminator; it is switched on by the second-level gateway when the tags need to be recharged and the duration of the illumination phase is properly determined so that tags can recover the energy consumed during the monitoring operation. This WPT phase will be called illumination in the following. During illumination, the different $G_{2|i}$ are emitting radio waves with high power on one of the frequency channels available in the 2.4 GHz band. It is worth noting that the illuminator transmits with a power considerably larger than the one used by the LoRa radio transceiver, which is upper-bounded to 12.5 dBm at 2.4 GHz [43]. Indeed, we suppose that each illuminator transmits WPT signals with a power level able to guarantee a received power of approximately -7 dBm, which is the minimum to let WPT working properly [44]. Considering the huge losses characterizing typical industrial scenarios (see the subsection III-D), the illuminator should transmit at least some tens of Watt.

C. The LoRaIN TDMA-FDMA Approach

Despite the (ideal) electromagnetic separation of adjacent machine sections, inter-cluster interference may still be present. Indeed, illumination in one cluster can interfere with the communication phase of another one, that is when tags transmit the measured data to their second-level gateway. Furthermore, inter-cluster interference may also happen between two (or more) simultaneous communication phases of different clusters. This subsection describes how the Time Division (TDMA) and Frequency Division Multiple Access (FDMA) approach of LoRaIN can solve these problems.

- *FDMA component of LoRaIN:* G_1 assigns a different LoRa channel in the 2.4 GHz band to each cluster. These channels are used for the communication phase. Therefore, tags belonging to different clusters can simultaneously transmit data to their second-level gateways without interfering with each other. In addition, clusters share others two frequency channels, one is used for illumination and the other for network formation (the latter is described in Section IV-C). Hence, among K available channels in the 2.4 GHz band, 2 are exploited by all clusters for illumination and network formation, while the remaining $K-2$ are uniquely assigned to clusters for communication purposes;
- *TDMA component of LoRaIN:* The fact that illumination and communication of different clusters are separated in frequency may, in principle, eliminate the inter-cluster interference that they produce. Nevertheless, the high powers used for illumination are such that the power amplifiers are forced to work in non-linear regions. Consequently, the signal emitted by each illuminator is not confined within a single LoRa channel and different side lobs on adjacent channels can be generated. Therefore, illumination of one cluster can still interfere with the communication of another one due to the presence of these unwanted side-lobs. As a countermeasure to this, clusters are synchronized, such that illumination and communication are also separated in time. This synchronization can be ensured by G_1, which can coordinate all $G_{2|i}$ operations in time by means of periodic packets sent in broadcast via PoE. These packets contain the indication of the action to be performed (communication or illumination), so that all clusters perform the same operation at the same time.
  Finally, when clusters are performing communication, intra-cluster interference may arise between tags that are transmitting their data to their second-level gateway. Therefore, LoRaIN also foresees an intra-cluster TDMA strategy which will be described in Section IV-B.

Due to the absence of inter-cluster interference for the reasons explained above, in the following, we will just focus on a single cluster managed by a $G_{2|i}$.

D. Statistical Path Loss Description

Automation machines are characterized by an harsh and complex environment, not easy to be modelled. In order to reproduce a realistic environment in the simulator, we have characterized the path loss experienced at 2.4 GHz through a measurement campaign over a real automation machine. To this aim, we used two LoRaIN boards: a second-level gateway and a single tag. The gateway was in a fixed position, while we moved the tag all over the machine, in 20 different locations. Figure 2 shows the fixed position of the gateway and one location of the tag (more details cannot be disclosed due to confidentiality reasons). In addition, experiments were conducted in two different conditions from the propagation viewpoint, since we have opened and closed the door through which the considered machine is accessible.

For each node location, we performed the following operations:

1) The second-level gateway is switched on and it immediately sets the reception mode;
2) The tag wakes up and it suddenly performs 2000 consecutive uplink transmissions of 10 bytes each, with power level $P_{\mathrm{T}} = -1\ dBm$;
3) Repetition of Step 2, after having closed the door of the machine.

Therefore, each location was characterized by 4000 values of received powers $P_{\mathrm{R_k}}$ (at gateway side), that is path loss, $PL_k = P_{\mathrm{T}} - P_{\mathrm{R_k}}$ (dB unit). The statistics of the path loss PL has been then computed, putting together measurements performed in the different positions and conditions (door open and closed).

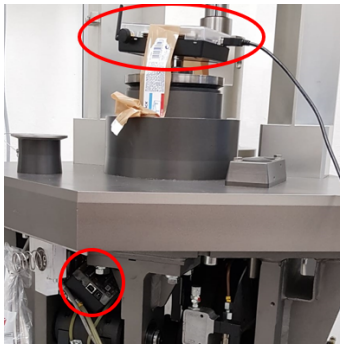

Fig. 2. Reference industrial machine used for the path loss characterization at 2.4 GHz, where the top-red circle highlights the second-level gateway, while the node is in the bottom-left corner.

In particular, it turned out that the probability mass function (pmf) of the measured path loss in linear unit, PL, resembles to a Rayleigh distribution, whose parameter coincides with the abscissa of the peak. The reader can refer to Appendix A for a complete description of the procedure we followed to achieve the aforementioned result.

This well-known shape of the pmf has simplified the implementation of our LoRaIN simulator, and each node can be associated to an instance of the Rayleigh-distributed path loss. Details of the simulator can be found in Appendix B.

IV. The Proposed Protocol Stack

A. PHY layer: LoRa at 2.4 GHz

As described in [45], LoRa is an M-ary digital modulation, where the M possible waveforms are chirp modulated signals over a given Bandwidth (BW). Four possible values of BW can be defined at 2.4 GHz: 203, 406, 812 and 1625 kHz. In all cases, the 2.4 GHz band has a number of frequency channels larger than ten (since its overall bandwidth is 80 MHz in most countries). M is an important degree of freedom, as it is given by $M = 2^{SF}$, where the Spreading Factor (SF) is an integer number ranging from 5 to 12. The larger the SF and the smaller will be the receiver sensitivity, but the longer will be the transmission time, called Time On Air (ToA). The latter is computed according to the following formula:

$$ToA = \frac{2^{SF}}{BW} \cdot N_{\mathrm{S}} \tag{1}$$

where N_{S} is a function of the SF and it can be written as in eq. (2), when Long Interleaving mode is not used [43].

A remark is that we use the LoRa Explicit (Variable-length) Header mode, which adds both the Cyclic Redundancy Check (CRC) and the header to the packet. This is the reason for the presence of N_{C} and N_{SH} in eq. (2), since they represent the number of bits for the CRC and the number of symbols for the header, respectively. We also use the default value for the number of symbols characterizing the LoRa preamble, denoted as N_{SP}. Their three values are listed in Section VI and they form the LoRa PHY header.

Moreover, the term U appearing in eq. (2) refers to the number of bytes of the LoRa PHY Service Data Unit (SDU), as shown in Figure 3 and described in details in subsection IV-B.

LoRa also envisions different Coding Rates (CR) values to trade reliability and ToA. We chose the lowest level of protection, that is a CR of 4/5. Such value implies that the term CR in eq. (2) is set to 1, as described in [43].

B. Upper layer: LoRaIN

This subsection will describe the protocol that is used by tags of the cluster, called LoRaIN as the network architecture in which it runs.

Time is organised into frames and each frame starts with a *Beacon* packet sent by $\mathrm{G}_{2|i}$ to tags in the cluster, to notify them regarding the actions to be taken. In particular, there exists two type of frames, both having the same duration: 1) *Default Frame*, used to keep tags synchronised; 2) *Reading Frame*, where tags have to take measurements for an interval T_{M} and send them to $\mathrm{G}_{2|i}$; in this case, the access to the channel is managed via a TDMA approach.

If no assignments are generated at the HMI, *Default Frames* come in succession: $\mathrm{G}_{2|i}$ periodically sends *Beacon-Default* packets, tags wake up for receiving the packet and then they go to sleep mode for the rest of the frame.

When a task assignment is performed at the HMI, the subsequent beacon will notify the tags regarding the beginning of the *Reading Frame*, sending a *Beacon-Comm-Read*. The *Reading Frame* structure is shown in Figure 4, and it is computed as:

$$T_{\mathrm{F}} = T_{\mathrm{B}} + T_{\mathrm{M}} + T_{\mathrm{C}} + T_{\mathrm{I}} \tag{3}$$

The different intervals of time in eq. (3) are listed below:

- T_{B}: Beacon time is the interval of time needed to transmit the *Beacon-Comm-Read* and the latter has the same duration of a *Beacon-Default*;
- T_{M}: Measuring time is the interval of time during which all tags are taking measures (acceleration and temperature in our case);
- T_{C}: Communication time is the portion of the *Reading Frame* which is dedicated to the transmission of the measurement results from tags to $\mathrm{G}_{2|i}$;
- T_{I}: Illumination time is the interval of time where nodes are in low-power mode while they are recharged by the illuminator.

It is important to underline that T_{F} also represents the duration of *Default Frames*, even if tags are in low-power mode throughout all the frame. Tags should be aware of the value of T_{F}, as well as all the timings appearing in eq. (3) , to be synchronized with $\mathrm{G}_{2|i}$. Such timings are retrieved from the beacons and they are used to re-set their internal clock, called Real-Time Clock (RTC), such that the synchronization is kept.

In the following, we provide more details about T_{C} and T_{I}. In fact, the values of T_{B} and T_{M} are fixed a-priori because the size of the *Beacon-Comm-Read*, as well as the requested duration of the measure, can be set independently on the number of tags present in the cluster. That is not the case for T_{C} and T_{I}, which are functions of N, that is the number of tags in the cluster.

$$N_{\mathrm{S}} = \begin{cases} N_{SP} + 6,25 + 8 + ceil\left(\frac{max(8\cdot U + N_C - 4\cdot SF + N_{SH}, 0)}{4\cdot SF}\right)\cdot(CR+4) & SF < 7 \\ N_{SP} + 4,25 + 8 + ceil\left(\frac{max(8\cdot U + N_C - 4\cdot SF + 8 + N_{SH}, 0)}{4\cdot SF}\right)\cdot(CR+4) & 7 \leq SF \leq 10 \\ N_{SP} + 4,25 + 8 + ceil\left(\frac{max(8\cdot U + N_C - 4\cdot SF + 8 + N_{SH}, 0)}{4\cdot (SF-2)}\right)\cdot(CR+4) & otherwise \end{cases} \quad (2)$$

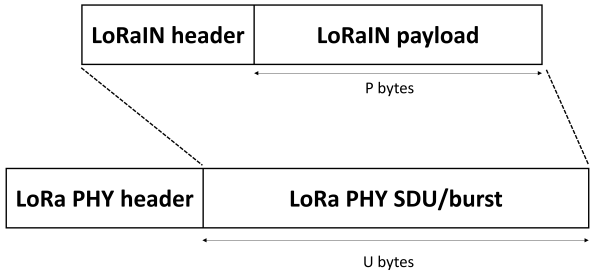

Fig. 3. LoRa Protocol (PDU) and Service Data Unit (SDU) format.

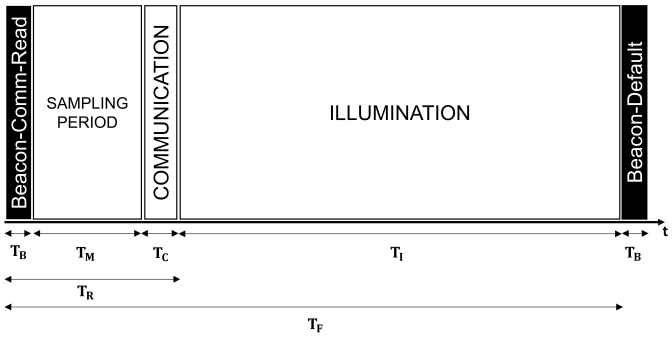

Fig. 4. The *Reading Frame* structure.

1) Computation of T_{C}: Each node is supposed to encode their measurements through a fixed amount of bytes, denoted as P; these bytes form the LoRaIN payload, which depends on the data measured by sensors on board. Moreover, it is added a LoRaIN header composed of 10 bytes, including the source and destination addresses (2 bytes each) as well as the network identifier (see Figure 3).

To simplify the notation, we will denote as *burst* the LoRa PHY SDU, composed of the LoRaIN payload and the LoRaIN header, and as *packet* the LoRa Protocol Data Unit (PDU), composed of the *burst* and the LoRa PHY header (the latter has been described in subsection IV-A).

The number of bytes included in the *burst* is denoted as U and the LoRa PHY layer cannot transmit more than $U_{\mathrm{M}} = 253$ bytes within a single transmission [43]; therefore, when T_{M} expires, each node requires n transmissions to transmit U bytes to $\mathrm{G}_{2|i}$, where the value of n is given by:

$$n = ceil\left(\frac{U}{U_{\mathrm{M}}}\right) \quad (4)$$

Each node will then transmit in n dedicated and consecutive time slots; in this way, intra-cluster interference is completely avoided.

TABLE I
VALUES OF RECEIVER SENSITIVITIES CORRESPONDING TO ALL POSSIBLE SPREADING FACTORS AT 2.4 GHZ, ASSUMING A BW OF 1625 KHZ

SF	P_{RS} [dBm]
5	-99
6	-103
7	-106
8	-109
9	-111
10	-114
11	-117
12	-120

The duration of each time slot depends on the value of U. In particular, two time slot durations are defined: $T_{\mathrm{S}|1}$ and $T_{\mathrm{S}|2}$, computed as follows:

$$T_{\mathrm{S}|1} = ceil\left(\frac{ToA_{\mathrm{M}}}{1 - \frac{T_{\mathrm{G}}}{100}}\right) \quad (5)$$

$$T_{\mathrm{S}|2} = ceil\left(\frac{ToA_{\mathrm{Y}}}{1 - \frac{T_{\mathrm{G}}}{100}}\right) \quad (6)$$

where $ceil()$ is a function which rounds the input to the nearest integer greater than or equal to that element; T_{G} is the percentage of guard time within a single slot; ToA_{M} is the LoRa Time on Air (ToA) related to a *burst* of U_{M} bytes (the maximum one), while ToA_{Y} refers to the remaining amount of bytes that should be transmitted in the last time slot, that is $Y = U - (n-1)\cdot U_{\mathrm{M}}$.

For example, if $U = 600$ bytes, then each node transmits a *burst* of 253 bytes for two times and $Y = 94$ bytes in the third time slot.

Finally, reminding that N is the number of nodes within a cluster, T_{C} is given by:

$$T_{\mathrm{C}} = N \cdot \left[(n-1)\cdot T_{\mathrm{S}|1} + T_{\mathrm{S}|2}\right] \quad (7)$$

It is worth noting that if $U \leq U_{\mathrm{M}}$, then each node transmits using a single time slot ($n = 1$) of duration $T_{\mathrm{S}|2}$, where ToA_{Y} of eq. (6) turns out to be ToA_{U}.

Obviously ToA_{M} and ToA_{Y} depend on the bit rate, which has an inverse proportionality with the spreading factor. In particular, the SF is set to the minimum value allowing connectivity between $\mathrm{G}_{2|i}$ and all tags in the cluster; in this regard, a node is considered connected if the received power exceeds the receiver sensitivity P_{RS}, whose values are taken from LoRa specifications and they are shown in Table I for the sake of completeness [43]. As it can be noted, larger SF

produce a lower receiver sensitivity and the latter should be compatible with the lowest level of received power in the cluster. In LoRaIN, the choice of SF is performed during the network formation phase, as described in subsection IV-C.

A final remark refers to the time slot scheduling: as we mentioned earlier, each time slot is dedicated to a single node, avoiding any interference among them. In fact, each node is associated to an address, and the latter is used in the *Beacon-Comm-Read* to tell the node when to start its transmission. Whenever one node is transmitting, all the others are waiting their turn in low-power mode. When a node has completed its transmission, it will be switched off until the end of T_{F}. This operation is performed by a hardware component mounted on tags, called Real-Time Clock (RTC). Nevertheless, the last-scheduled node has the highest power consumption because it has to wait all the other transmissions. For the sake of fairness, the last-scheduled node is not always the same since $G_{2|i}$ randomly scramble the mapping between time slots and node addresses at each *Beacon-Comm-Read*.

2) Computation of T_{I}: The value of T_{I} is chosen so that tags can recover the energy they have consumed during T_{B}, T_{M} and T_{C}. The sum of these three terms is called Round Trip Time (RTT), because it represents the interval of time elapsing from the transmission of the *Beacon-Comm-Read* and the reception of the last-scheduled *packet* (see Figure 4). We will denote it as T_{R} hereafter.

At the beginning of T_{I}, $\mathrm{G}_{2|i}$ switches on the illuminator and the tags start to be recharged. Each tag consumes a different amount of energy in T_{C}, because the time it should wait in low-power mode depends on its address. However, T_{I} is computed considering the largest amount of energy consumed in the cluster, which belongs to the last-scheduled node (the N-th one), since it is the last node which is switched on by its own RTC. Therefore, the expression of T_{I} is as follows:

$$T_{\mathrm{I}} = \frac{E_{\mathrm{N}}}{P_{\mathrm{A}}} = \frac{E_{\mathrm{N}}}{\eta \cdot P_{\mathrm{R_m}}} \tag{8}$$

where E_{N} is the energy consumed by the N-th node and its expression is reported in subsection V-A, $P_{\mathrm{R_m}}$ is the minimum received power during illumination phase, P_{A} is the minimum absorbed power and it is a fraction (η) of the minimum received power ($P_{\mathrm{R_m}}$). It is worth noting that the absorbed power should be intended as Direct Current (DC) power, while $P_{\mathrm{R_m}}$ is the Radio Frequency (RF) power available at the receiving antenna input port [44].

C. LoRaIN Network Formation

For the sake of completeness, this subsection briefly describes how the LoRaIN network is formed, that is the procedure with which nodes associate to a given cluster.

1) When the network has to be created, all $\mathrm{G}_{2|i}$ wait in reception on the common channel dedicated to the network formation phase, until G_1 indicates that this phase can finish and the system can start the normal operations that have been described in the previous subsection. To maintain time synchronization with the tags that are already in the network, each $\mathrm{G}_{2|i}$ continues to send *Beacon-Default* with periodicity T_{F} on the frequency channel dedicated to the considered cluster. In this phase, no *Reading Frames* are possible. Each $\mathrm{G}_{2|i}$ uses two transceivers simultaneously on two different frequency channels, one (the common one) in reception of association requests, and the other (the dedicated one) in transmission of *Beacon-Defaults*. For the sake of brevity, we will call the transceiver using the former as *common* transceiver, since it works on a channel which is shared by all clusters;
2) When a new tag requests to be associated to the network, it will send an *Association-Request* packet on the aforementioned common channel, indicating its willingness to be connected. The SF used for this packet is the highest one to maximize the coverage range of the network (that is 12 at 2.4 GHz [43]);
3) The association packet is received by all $\mathrm{G}_{2|i}$ for which the received power level is above the receiver sensitivity provided by $SF = 12$ (see Table I). In particular, each of these $\mathrm{G}_{2|i}$ sends to G_1 the corresponding received power level so that the first-level gateway can choose the second-level gateway that has received the *Association-Request* with the highest power level.
4) G_1 compares the selected received power level with the receiver sensitivities provided by LoRa at 2.4 GHz in order to choose the lowest possible SF that can be used by the considered cluster. Then, the first-level gateway will compare the newly computed SF with the one that the cluster is already using (if any) and it selects the highest one. This is a worst case scenario, because the choice is influenced by the tag of the cluster from which the lowest received power has been received. Once this computation ends, G_1 notifies its choice to all $\mathrm{G}_{2|i}$ which was involved in the selection and the chosen one will then answer to the tag with an *Association-Response* packet containing: the assigned address, the frequency channel used by the chosen cluster, the time left until the next *Beacon-Default* will be transmitted on that frequency channel and the SF to be used.

When G_1 receives from the HMI the command that ends the network formation phase, it will send a notification to all $\mathrm{G}_{2|i}$ such that they can switch off their *common* transceiver.

V. Performance evaluation

In this Section we describe the key performance indicators (KPI) characterizing LoRaIN, while their numerical values are shown in Section VI as a function of different input settings.

A. Energy Consumption

An important figure of merit is the energy consumed by a tag during the *Reading Frame*; this metric is used to compute the illumination time T_{I}, as described in subsection IV-B.

We will denote this energy as E_j, and it will be the energy spent by the j-th node during T_{R}, where j spans from 1 to

N. The expression of E_j is shown in eq. (9).

$$\begin{aligned} E_j \ = & P_{\mathrm{RX}} \cdot T_{\mathrm{B}} + P_{\mathrm{M}} \cdot T_{\mathrm{M}} + \\ & + P_{\mathrm{L}} \cdot (j-1) \cdot [(n-1) \cdot T_{\mathrm{S}|1} + T_{\mathrm{S}|2}] + \\ & + P_{\mathrm{TX}} \cdot [(n-1) \cdot ToA_{\mathrm{M}} + ToA_{\mathrm{Y}}] + \\ & + P_{\mathrm{L}} \cdot (n-1) \cdot (T_{\mathrm{S}|1} - ToA_{\mathrm{M}}) \end{aligned} \tag{9}$$

where:

- the first term is the energy spent for receiving the *Beacon-Comm-Read*, being P_{RX} the power spent in reception;
- the second term is the energy spent during the measurement, being P_{M} the power consumed when the sensors are sampling;
- the third term is the energy spent when the node is waiting the beginning of its slot, being P_{L} the power consumed in low-power mode;
- the fourth term is the energy spent for the transmission of the *packets*, being P_{TX} the power spent in transmission;
- the last term is the energy spent during the guard time portion of each time slot, where the node is not transmitting and it can be in low-power again.

In eq. (9) we assume zero energy consumption during the illumination portion of the *Reading Frame* (see Figure 4). This is possible thanks to the ultra-low power features of commercial RTCs[3], being the unique hardware component of the node which is consuming during T_{I}.

Furthermore, eq. (9) assumes that all nodes are perfectly synchronized, thanks to the presence of a guard time in each time slot, denoted as T_{G}, ensuring no intra-cluster interference. Since the lack of this hypothesis could negatively affect the LoRaIN performance, our simulator also implements a random clock drift, according to which one tag can loose synchronization with the $\mathrm{G}_{2|i}$ and transmits simultaneously with another one (see subsection V-B).

We then introduce the average energy consumption $\overline{E}$, averaged among the tags, that is $\overline{E} = \frac{\sum_{j=1}^{N} E_j}{N}$.

B. Success Rate

As anticipated in subsection V-A, our simulator can assess the LoRaIN performance even if the clocks mounted on tags are shifted with respect to the exact timing taken by $\mathrm{G}_{2|i}$. This may be a problem of real-world implementations, since IoT devices should be low-cost and their clocks are then limited in precision.

More specifically, we assume that all tags have the same clock, whose precision is expressed in Parts Per Million (ppm). It is well-known that, if a tag has to count an interval T, its effective value will be $T + \Delta T$, where:

$$\Delta T \ = \ \pm\, T \cdot ppm \cdot 10^{-6} \tag{10}$$

This possibility may lead to partial or total collisions, since the transmissions of two or more tags may partially or totally overlap in time domain.

[3]An example of RTC data sheet can be found at: https://abracon.com/Precisiontiming/AB18X5-RTC.pdf

For the sake of simplicity, we did not implement a capture effect; in particular, a *packet* is correctly received if only the *burst* has collided. Conversely, if the collision has involved the LoRa PHY header, the *packet* is considered lost. It immediately follows that we can define a success rate $\overline{S_{\mathrm{R}}}$ as an average of the successful node transmissions, that is: $\overline{S_{\mathrm{R}}} = \frac{\sum_{j=1}^{N} S_{\mathrm{R_j}}}{N}$, where $S_{\mathrm{R_j}}$ is the percentage of *packets* successfully transmitted by the j-th node.

C. Network Throughput

The average network throughput $\overline{S}$, when considering a cluster composed of N tags, is given by:

$$\overline{S} \ = \ \frac{N \cdot P}{T_{\mathrm{F}}} \cdot \overline{S_{\mathrm{R}}} \tag{11}$$

where we assume that no connectivity issues are present between tags and $\mathrm{G}_{2|i}$. The latter is possible thanks to the fact that $\mathrm{G}_{2|i}$, during the formation of the network, selects the value of SF to be used by all tags in the cluster based on the tag characterized by the lowest level of received power (see subsection IV-C).

It is worth noting that $\overline{S_{\mathrm{R}}} = 1$ if the clock shifts are negligible compared to the timings to be counted by tags. In particular, Section VI will show the robustness of LoRaIN, since only unrealistic values of ppm can produce a reduction of the nominal values of $\overline{S}$.

D. Latency

We define the LoRaIN latency as the average time that an operator should wait before seeing the result of the monitoring operation at the HMI, that represents a way to quantify the LoRaIN responsiveness. Hence, the latency is determined by the waiting time of the last-scheduled node, since the data are displayed at the HMI as long as all nodes have transmitted.
It is worth noting that the operator request is asynchronous, and it can happen in a random instant of a *Default Frame*. The system immediately perceives the request, but the *Reading Frame* can only start at the end of the current *Default Frame*. Considering a generic request, we define the LoRaIN latency, L, as follows:

$$L = T_{\mathrm{F}} - U_{\mathrm{R}} + T_{\mathrm{R}} \tag{12}$$

where U_{R} is the instant in which the request is generated by the user, and it is modelled as an uniform random variable within the range [0, T_{F}].

The reader can better understand eq. (12) by looking at Figure 5, where it is shown an example of two different requests, appearing at random instants U_{R}^1 and U_{R}^2 and characterized by two different latencies L_1 and L_2.

VI. Results and Discussion

In this Section we present and discuss some results spreading out from the LoRaIN simulator, with the ambition of quantifying the robustness, scalability and responsiveness of LoRaIN. To this aim, all the KPIs introduced in Section V are numerically evaluated as a function of different input

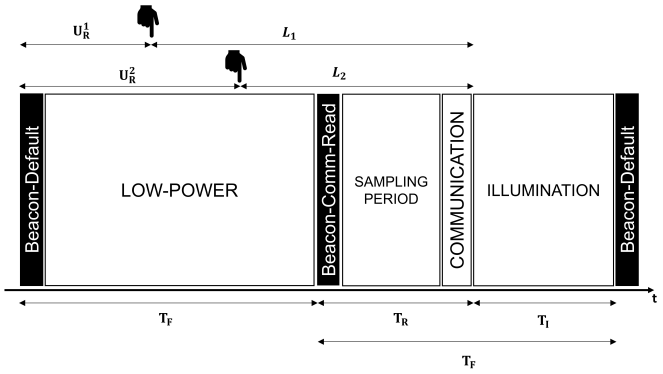

Fig. 5. An example of two monitoring requests appearing at random instants U_{R}^1 and U_{R}^2 and characterized by two different latencies L_1 and L_2.

TABLE II
PARAMETER SETTINGS

Parameter	Value	Parameter	Value
BW	1625 kHz	η	0.4
CR	$4/5$	P_{Rm}	-7 dBm
N_{C}	16 Bits	P_{RX}	32.3 mW
N_{SH}	20 Symbols	P_{M}	0.252 mW
N_{SP}	12 Symbols	P_{L}	0.528 mW
L_{H}	10 Bytes	P_{TX}	99 mW
T_{M}	0.5 s	N_{F}	10000

parameters. All results have been obtained by averaging over a number N_{F} of transmissions, that is *Reading Frames*, and this also means that L of eq. (12) becomes $\overline{L} = T_{\mathrm{F}} - \overline{U_{\mathrm{R}}} + T_{\mathrm{R}}$, where $\overline{U_{\mathrm{R}}} = T_{\mathrm{F}}/2$. However, more details about the simulator can be found in Appendix B.

System parameter settings, if not otherwise specified, are reported in Table II. In particular:

- The chosen value of BW is the maximum one at 2.4 GHz; hence, the system works with the largest possible bit rate for a given SF and this aspect is important to shrink the LoRaIN latency as much as possible;
- We used the smallest value of CR, since no interference is theoretically present in LoRaIN, thanks to the FDMA-TDMA approach. Moreover, this value allows a good resilience with respect to Wi-Fi interference, as shown in the final part of this Section;
- For conciseness, we denote with L_{H} the 10 bytes of LoRaIN header. Moreover, the *burst* characterizing each *Beacon-Comm-Read* is of 10 bytes too, since it does not embed a LoRaIN payload. This is possible by using one bit of the LoRaIN header to let nodes discriminate between *Beacon-Default* and *Beacon-Comm-Read*;
- During illumination phase, the recharging operation of nodes is characterized by an RF-to-DC efficiency, η, which is an increasing function of the RF power received by nodes during illumination phase. To allow a sufficient energy recovery to all nodes in the cluster, we design T_{I} by considering the minimum RF received power in the cluster, namely $P_{\mathrm{R_m}}$. However, we assume that η is 0,4 for all tags, which means that $P_{\mathrm{R_m}}$ is approximately -7 dBm, as shown in [44]. This is compatible with the losses we have measured (see Appendix A), since the illuminator is supposed to transmit with a sufficiently high power for the scenario of interest;
- The devices used in the real implementation are custom boards made of different hardware components. Therefore, the values of consumed powers appearing in Table II are taken by jointly considering their data sheets, that are [43], [46], [47], [48]. One remark is that P_{L} is larger than P_{M} because our physical implementation foresees that sensors mounted on tags work in a lower voltage regime than the rest of the board.

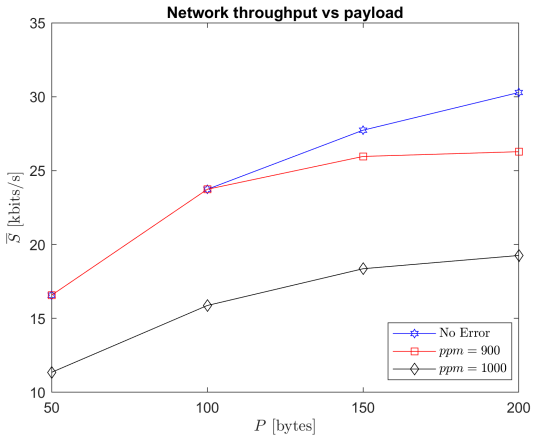

Fig. 6. Network throughput as a function of the payload for different values of ppm characterizing the clocks mounted on tags.

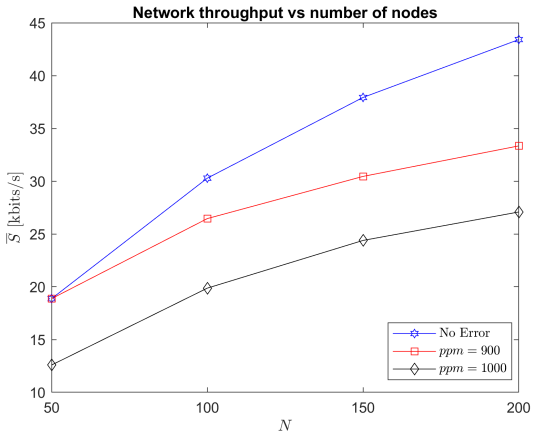

Fig. 7. Network throughput as a function of the number of nodes for different values of ppm characterizing the clocks mounted on tags.

A first result is depicted in Figure 6, where the growing trend of S with P is confirmed, considering a cluster formed by $N = 100$ nodes. The transmit power of the LoRa communications, P_{T}, has been set to its maximum value of 12.5 dBm, allowing to use the minimum SF in the scenario of interest (see Appendix A for details on path loss model). With SF 5, T_{B} can be set to 2 ms and we consider no guard time, that is $T_{\mathrm{G}} = 0\%$, to force a tight synchronization among nodes.

Three different cases have been simulated: i) when no

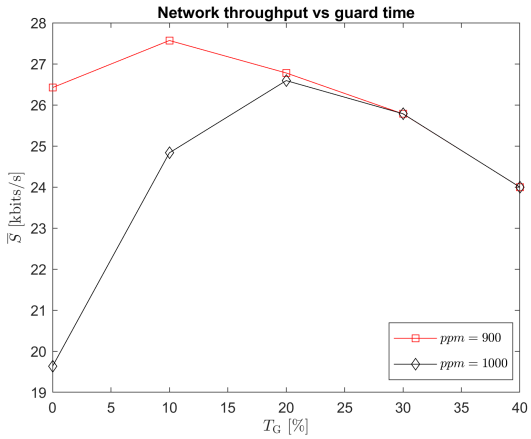

Fig. 8. Network throughput as a function of the guard time for different values of ppm characterizing the clocks mounted on tags.

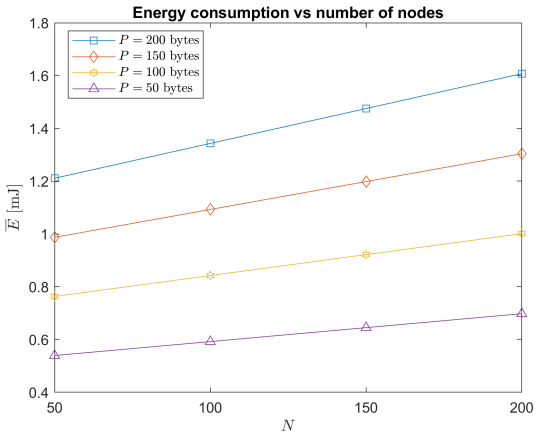

Fig. 9. Energy consumption as a function of the number of nodes and for different values of LoRaIN payload P.

synchronization error is present (clocks on nodes are ideal), ii) when nodes mount clocks with a ppm of 1000 and iii) when ppm is 900. It is clearly evident that a decrease of network throughput only happens for unrealistic values of ppm (the latter is typically a few tens), demonstrating the robustness of LoRaIN to intra-cluster interference. The reason of these improbable values of ppm can be found in eq. (10), since the clock shifts are also proportional to the intervals of time to be counted and LoRaIN foresees timings of few hundreds of ms in the worst case.

Furthermore, considering the same three cases of clock shifts, and assuming a LoRaIN payload of 200 bytes, Figure 7 shows that the network throughput grows with N albeit the impact of clock shifts is larger for crowded clusters, due to longer timings to be counted. In fact, the larger is N and the longer is the waiting time for the last-scheduled node, before it can actually transmit its data. This result suggests that violations of intra-cluster interference do not limit the scalability of LoRaIN. Both Figure 6 and 7 consider a $T_G = 0\%$ because the aim is to emphasize the effect of the intra-cluster interference. However, the value of T_G should be carefully chosen for a given clock precision (ppm value); indeed, the longer the guard time, the lower is the collision probability but T_F enlarges as well (see eq. (5), (6), (7) and (3)). Therefore, the network throughput as a function of the guard time is subject to a trade-off, because its value increases with T_G as long as the increase in the denominator of S (that is T_F) does not become dominant. This trend is confirmed in Figure 8, where the network throughput is depicted as a function of the guard time for two values of ppm (900 and 1000) and considering $N = 100$ and $P = 200$ bytes. It is interesting to note that the optimum value of T_G is different if the clock precision changes. Figure 8 shows that the network throughput is maximized for $T_G = 10\%$ and $T_G = 20\%$, in case of $ppm = 900$ and $ppm = 1000$, respectively. This result is in line with our expectations, since a better clock precision reduces the collision probability and thus the increase of the guard time becomes less useful for the network throughput viewpoint. Moreover, the reader can note that the two curves converge when the guard time is so high that collisions do not occur anymore.

Regarding the low-power needs of IIoT applications, Figure 9 reports the average energy consumption, $\overline{E}$, as a function of the number of nodes N, by varying the LoRaIN payload from 50 to 200 bytes. These values of P are sufficient for many IIoT applications and the differences in terms of average energy consumed are of at most 1 mJ, demonstrating how LoRaIN is able to exploit the low-power features of the LoRa technology. However, in opposition to Figures 6 and 7, in this simulation we have set $T_G = 10\%$ to be much closer to our physical implementation.

However, the choice of the spreading factor also affects the energy consumption of nodes and thus it changes the time needed to recharge them. In fact, larger spreading factor implies a higher power consumption, since the same *packet* is transmitted in longer time. In this regard, Figure 10 shows the impact of two different spreading factors on the illumination time T_I, which is plotted as a function of the number of nodes in the cluster and considering a LoRaIN payload of 100 bytes. The curves confirm the growth of T_I for larger SF; more specifically, the value of $SF = 5$ has been obtained assuming $P_T = 12.5$ dBm (the maximum one), while $SF = 6$ is set when $P_T = -18$ dBm (the minimum one). Indeed, in the latter case, some nodes are not connected to the second-level gateway and $G_{2|i}$ should then increase the SF from 5 to 6. One can also notice that tags are recharged in less than 6 seconds even for clusters hosting 200 nodes and transmitting 100 bytes each, thus showing a good scalability property for the scenario of interest. These numbers are in line with what we experienced on-field during the PoC, since we had 5 nodes that were recharged in less than 2 seconds.

Figure 11 shows the variations of the LoRaIN latency with the number of nodes N, for representative LoRaIN payloads of 100 and 200 bytes. Without loss of generality, we assume that the propagation delays of the wired connections are negligible. As it can be seen, considering a crowded cluster of 200 nodes, the operator has to wait (on average) no more than 7 seconds, which seems to be a reasonable value for the

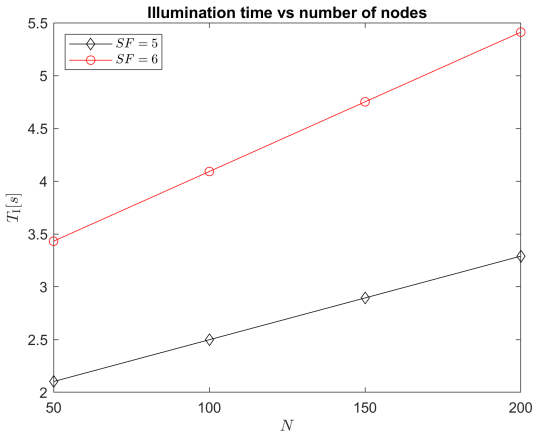

Fig. 10. Illumination time as a function of the number of nodes and for two different values of SF.

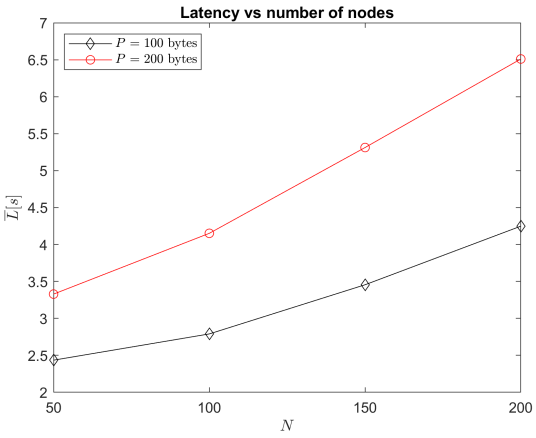

Fig. 11. Latency as a function of the number of nodes and for different values of P.

human perception. Furthermore, by considerably increasing the precision of the measurements taken by tags, which ends-up in doubling the value of P, the LoRaIN responsiveness increases of less than 3 seconds in the worst case, showing a large degree of flexibility for the customer viewpoint.

Finally, we study the robustness of the system with respect to the interference generated by an IEEE 802.11g network, working on the same 2.4 GHz band. For experiments we have used a TP-Link TL-WA830RE access point (AP), configured to work in IEEE 802.11g mode with maximum available transmit power and a maximum rate allowed of 54 Mbit/s. To generate a constant Wi-Fi occupancy we used two laptops working as video streaming client and server (VLC Media player was running at both laptops). An HTTP (HyperText Transfer Protocol) server was set up to broadcast an mp4 video in on-demand fashion. The experimental setup is shown in Fig. 12: Server and AP were connected exploiting an Ethernet cable, while the client was communicating to the AP via the wireless connection enabled by IEEE 802.11g. As for the LoRaIN devices, we considered one transmitter (LoRaIN tag) and one receiver (G_2) at a distance of 3.2 m and both devices were at an height of 0.5 m from the floor, while G_2 was located

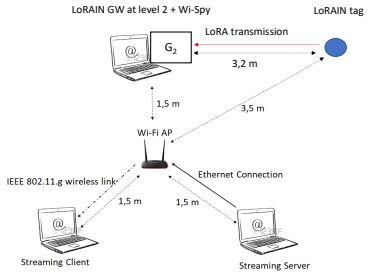

Fig. 12. Interference Evaluation: Experimental setup.

at 1.5 m from the AP.

In order to characterize the interference level suffered by the LoRa receiver, we estimated the Signal-to-Interference Ratio (C/I) as follows. A Wi-Spy device was located near G_2 to measure the interfering power, I, while the useful received power, C, was directly measured by the LoRa receiver of G_2, using the received signal strength indicator (RSSI). Finally, we used the Chanalyzer to measure the channel utilization, defined as the percentage of time the received signal was above a threshold of -105 dBm in the considered channel for a given interval of time (set equal to the duration of a single experiment). The packet success rate, S_R, was computed considering the transmission of 1000 packets.

In Table III we show S_R for different values of C/I. The channel occupancy was 20%. The carrier frequency of LoRaIN signal was set to 2.452 GHz, that is the central frequency of channel 9 used by the IEEE 802.11g network (completely overlapped channels). As can be seen, by increasing SF the time on air increases, bringing to larger collision probability, until a given value ($SF > 8$), where performance improve thanks to a modulation which is more robust to interference. However, as an example, setting $SF = 9$ in a LoRaIN cluster made of 50 nodes will bring to an average network throughput equal to 1.68 kbits/s. Conversely, the average network throughput increases up to 12.8 kbits/s if we set $SF = 5$ (see Figure 7), due to the notable decrease of the illumination time. Therefore, $SF = 5$ is the best choice to reach a trade-off between robustness with respect to Wi-Fi interference and energy consumption constraints. Finally, it is important to underline that measurements have been performed in a worst case scenario (completely overlapped channels, Wi-Fi AP at 1.5 meters in line-of-sight conditions), rarely occurring in a real premise, where tags are mounted into closed and well isolated industrial machines.

VII. Conclusions

In this paper we have proposed a communication protocol and architecture based on LoRa at 2.4 GHz, suitable for monitoring of industry machines.

LoRaIN provides a network throughput close to 25 kbit/s when 100 tags are deployed per cluster and each of them uses 100 bytes to encode measurements. For the same tag density,

TABLE III
PACKET SUCCESS PROBABILITY IN THE PRESENCE OF WI-FI INTERFERENCE.

SF	$C/I = -30$ **dB**	$C/I = -34$ **dB**
5	0,85	0,775
6	0,79	0,74
7	0,8	0,76
8	0,95	0,875
9	0,975	0,96
10	1	0,975
11	1	1
12	1	1

with a realistic values of WPT efficiency, the reaction time of the protocol is in the order of few seconds; such values are compatible with monitoring applications where humans are in the loop. On the other hand, for different machines, the WPT technique may require larger illumination times and protocol performance in terms of delays and network throughput may be worse.

LoRaIN has been implemented in a real-world context. The pilot project ends-up with a PoC made of few nodes and for this reason results are not compared to those presented here; in fact, we wanted to discuss the interference-agnostic properties of LoRaIN, as well as its scalability and responsiveness, on the basis of simulation results. However, the simulator has been designed starting from real-world measurements, thus producing results close to reality.

APPENDIX A
STATISTICAL PATH LOSS DESCRIPTION

Section III-D describes the procedure we followed to perform path loss measurements in the scenario of interest.

In particular, the pmf of path loss is computed considering the 80000 samples of losses generated by the measurements, PL_k, considering 20 tag positions, 2 conditions (door open and closed) and 2000 transmissions per position and scenario, and setting a discretization interval equal to $\frac{PL_{\max}-PL_{\min}}{1000}$, where $PL_{\max}$ and $PL_{\min}$ are the maximum and minimum values of measured loss, respectively. By displaying on an x-axis the representative path loss values of each discretization interval, and the corresponding pmf on the y-axis, the resulting plot is shown in Figure 13.

It is worth noting that the pmf resembles to a Rayleigh distribution, rather than Negative Exponential, because the first representative value of path loss in linear unit is pretty far from 0, contrarily to what it seems from Figure 13. To avoid any doubt, we have highlighted the first point of the pmf with the text-box in the top-left corner, while a zoomed version of the decreasing trend appears in the dashed square.

In our LoRaIN simulator, described in Appendix B, we obtain a Rayleigh random variable as $\sqrt{X^2+Y^2}$ where X and Y are zero-mean Gaussian random variables. In particular, we have set the standard deviation of both of them as the path loss value for which there is the peak of the measured Rayleigh pmf, as well-known from statistic theory.

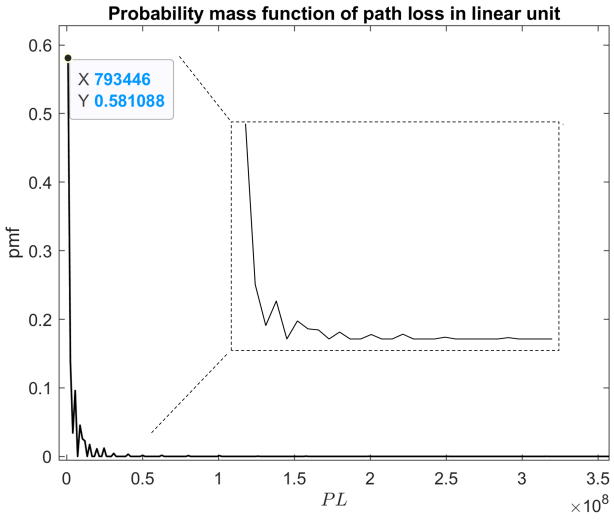

Fig. 13. Measured probability mass function of path loss in linear unit, resembling to a Rayleigh distribution (a zoomed version of the decreasing trend is depicted in the dashed square).

APPENDIX B
LORAIN SIMULATOR

Our LoRaIN simulator is discrete-time and it has been written in C. Each simulation is made of N_{F} steps and each of them corresponds to an entire *Reading Frame*. We call *Tick* the smallest interval of time foreseen within a *Reading Frame*, so that the latter can be subdivided in an (integer) number of *Ticks* (see Figure 14).

More specifically, the LoRaIN simulator performs the following macro-operations for each single step:

1) It assigns a path loss value to each node, using the Rayleigh distribution described in Appendix A;
2) It computes the received power of each node in the cluster as the difference in dB between the value of transmit power used by the LoRa transceiver, P_{T}, and the path loss associated to the node. Then it sets the SF to the minimum value for which the receiver sensitivity is lower than the minimum received power in the cluster;
3) It computes the LoRa TimeOnAirs (at 2.4 GHz) so that it obtains T_{B}, $T_{\mathrm{S}|1}$ and eventually $T_{\mathrm{S}|2}$ to match the requested T_{G};
4) It chooses the minimum between T_{B}, T_{S}, $T_{\mathrm{S}|1}$ and $T_{\mathrm{S}|2}$ (if present), to compute the *Tick*;
5) It simulates the communication part of the *Reading Frame* using a *Tick* discretization;
6) Having all the consumed energies from the previous step, it can compute $\overline{E}$, T_{I} and then T_{F};
7) It computes $\overline{S}$ before ending the simulation of the current step.

For the sake of simplicity, all timings, including the *Tick*, are rounded to integer numbers.

As far as the outputs are concerned, the simulator computes the metrics described in Section V for N_{F} times, but it finally displays their averages over N_{F}, which are those reported in Section VI. In fact, each node is characterized by a structure,

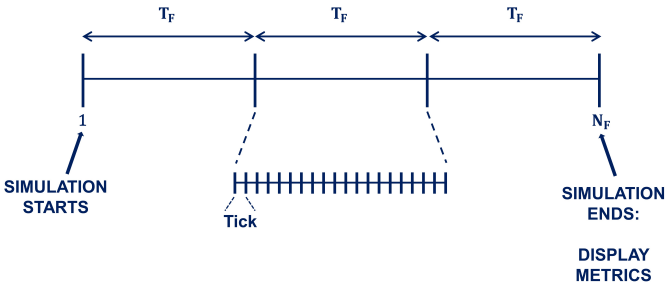

Fig. 14. Discrete-time structure of the LoRaIN simulator.

```
case Rx:
    if (t == nodes[i].timings.T)
    {
        // Metrics update
        nodes[i].metrics.nPacketsRx++;
        if (nodes[i].isReceiving == true)
        {
            nodes[i].metrics.nSuccessfullRx++; // Good reception
        }
        else
        {
            nodes[i].isReceiving = true; // Packet has not been received
        }
```

Fig. 15. Portion of the LoRaIN simulator where the counters for the Success Rate computation are updated.

which provides information about its state (transmission, reception, low-power, etc..) and it stores the number of *Ticks* that should elapse before changing state. During each *Tick*, the simulator checks the status of each node and it updates the metrics accordingly, such as the energy consumed. Before the *Tick* ends, it will update the state of each node, if necessary. For example, Figure 15 shows a portion of code where the simulator updates the counters used for the Success Rate computation, when the j-th node has to leave the reception state. The reader can also notice the variable " T " in the nodes' structure, which is used to know when the node has to change state, and the boolean "isReceiving", which is set to false when the collision is harmful because it has involved the LoRa PHY header.

A final remark is about what differentiate the simulation steps (simulated *Reading Frames*):

1) The path loss experienced by each single node, since the instances of the Rayleigh random variable are recomputed at each step;
2) The clock shift relative to the timings counted by each node, since the sign of eq. (10) is modelled as a discrete random variable with two equiprobable events;
3) The instant in which the operator has requested the monitoring operation, which is modelled as an uniform random variable which ranges between 0 and T_F.

REFERENCES

[1] C. Lu, A. Saifullah, B. Li, M. Sha, H. Gonzalez, D. Gunatilaka, C. Wu, L. Nie, and Y. Chen, "Real-Time Wireless Sensor-Actuator Networks for Industrial Cyber-Physical Systems," *Proceedings of the IEEE*, vol. 104, no. 5, pp. 1013–1024, May 2016.

[2] H. S. Kang, J. Y. Lee, S. Choi, H. Kim, J. H. Park, J. Y. Son, B. H. Kim, and S. Do Noh, "Smart manufacturing: Past research, present findings, and future directions," *International journal of precision engineering and manufacturing-green technology*, vol. 3, no. 1, pp. 111–128, 2016.

[3] P. Zheng, Z. Sang, R. Y. Zhong, Y. Liu, C. Liu, K. Mubarok, S. Yu, X. Xu *et al.*, "Smart manufacturing systems for Industry 4.0: Conceptual framework, scenarios, and future perspectives," *Frontiers of Mechanical Engineering*, vol. 13, no. 2, pp. 137–150, 2018.

[4] H. Yang, S. Kumara, S. T. Bukkapatnam, and F. Tsung, "The internet of things for smart manufacturing: A review," *IISE Transactions*, vol. 51, no. 11, pp. 1190–1216, 2019.

[5] S. Robla-Gómez, V. M. Becerra, J. R. Llata, E. Gonzalez-Sarabia, C. Torre-Ferrero, and J. Perez-Oria, "Working together: A review on safe human-robot collaboration in industrial environments," *IEEE Access*, vol. 5, pp. 26 754–26 773, 2017.

[6] J. R. Moyne and D. M. Tilbury, "The Emergence of Industrial Control Networks for Manufacturing Control, Diagnostics, and Safety Data," *Proceedings of the IEEE*, vol. 95, no. 1, pp. 29–47, 2007.

[7] A. Flammini, P. Ferrari, D. Marioli, E. Sisinni, and A. Taroni, "Wired and wireless sensor networks for industrial applications," *Microelectronics journal*, vol. 40, no. 9, pp. 1322–1336, 2009.

[8] J. García-Morales, M. C. Lucas-Estañ, and J. Gozalvez, "Latency-sensitive 5G RAN slicing for industry 4.0," *IEEE Access*, vol. 7, pp. 143 139–143 159, 2019.

[9] S. K. Rao and R. Prasad, "Impact of 5G technologies on industry 4.0," *Wireless personal communications*, vol. 100, no. 1, pp. 145–159, 2018.

[10] J. Cheng, W. Chen, F. Tao, and C.-L. Lin, "Industrial IoT in 5G environment towards smart manufacturing," *Journal of Industrial Information Integration*, vol. 10, pp. 10–19, 2018.

[11] K.-H. Chang, "Bluetooth: a viable solution for IoT?[Industry Perspectives]," *IEEE Wireless Communications*, vol. 21, no. 6, pp. 6–7, 2014.

[12] R. Tei, H. Yamazawa, and T. Shimizu, "BLE power consumption estimation and its applications to smart manufacturing," in *2015 54th Annual Conference of the Society of Instrument and Control Engineers of Japan (SICE)*. IEEE, 2015, pp. 148–153.

[13] A. Aijaz, "High-Performance Industrial Wireless: Achieving Reliable and Deterministic Connectivity over IEEE 802.11 WLANs," *IEEE Open Journal of the Industrial Electronics Society*, vol. 1, pp. 28–37, 2020.

[14] G. Cena, S. Scanzio, and A. Valenzano, "Seamless Link-Level Redundancy to Improve Reliability of Industrial Wi-Fi Networks," *IEEE Transactions on Industrial Informatics*, vol. 12, no. 2, pp. 608–620, 2016.

[15] L. Polak and J. Milos, "Performance analysis of LoRa in the 2.4 GHz ISM band: coexistence issues with Wi-Fi," *Telecommunication Systems*, pp. 1–11, 2020.

[16] P. Sommer, Y. Maret, and D. Dzung, "Low-Power Wide-Area Networks for Industrial Sensing Applications," in *2018 IEEE International Conference on Industrial Internet (ICII)*. IEEE, 2018, pp. 23–32.

[17] Morin, Elodie and Maman, Mickael and Guizzetti, Roberto and Duda, Andrzej, "Comparison of the device lifetime in wireless networks for the internet of things," *IEEE Access*, vol. 5, pp. 7097–7114, 2017.

[18] Kurtoglu, Abdullah and Carletta, Joan and Lee, Kye-Shin, "Energy consumption in long-range linear wireless sensor networks using LoRaWan and ZigBee," in *2017 IEEE 60th International Midwest Symposium on Circuits and Systems (MWSCAS)*. IEEE, 2017, pp. 1163–1167.

[19] Kwon, Dongwon and Rincón-Mora, Gabriel A and Torres, Erick O, "Harvesting kinetic energy with switched-inductor DC-DC converters," in *Proceedings of 2010 IEEE International Symposium on Circuits and Systems*. IEEE, 2010, pp. 281–284.

[20] P. D. Mitcheson, E. M. Yeatman, G. K. Rao, A. S. Holmes, and T. C. Green, "Energy harvesting from human and machine motion for wireless electronic devices," *Proceedings of the IEEE*, vol. 96, no. 9, pp. 1457–1486, 2008.

[21] Zeng, Yong and Clerckx, Bruno and Zhang, Rui, "Communications and signals design for wireless power transmission," *IEEE Transactions on Communications*, vol. 65, no. 5, pp. 2264–2290, 2017.

[22] B. Clerckx, R. Zhang, R. Schober, D. W. K. Ng, D. I. Kim, and H. V. Poor, "Fundamentals of wireless information and power transfer: From RF energy harvester models to signal and system designs," *IEEE Journal on Selected Areas in Communications*, vol. 37, no. 1, pp. 4–33, 2018.

[23] L. Tessaro, C. Raffaldi, M. Rossi, and D. Brunelli, "LoRa performance in short range industrial applications," in *2018 International Symposium on Power Electronics, Electrical Drives, Automation and Motion (SPEEDAM)*. IEEE, 2018, pp. 1089–1094.

[24] K. Mikhaylov, J. Petäjäjärvi, and J. Janhunen, "On lorawan scalability: Empirical evaluation of susceptibility to inter-network interference," in

2017 European Conference on Networks and Communications (EuCNC). IEEE, 2017, pp. 1–6.
[25] K. Mikhaylov, J. Petaejaejaervi, and T. Haenninen, "Analysis of capacity and scalability of the lora low power wide area network technology," in *European Wireless 2016; 22th European Wireless Conference*. VDE, 2016, pp. 1–6.
[26] F. Van den Abeele, J. Haxhibeqiri, I. Moerman, and J. Hoebeke, "Scalability analysis of large-scale lorawan networks in ns-3," *IEEE Internet of Things Journal*, vol. 4, no. 6, pp. 2186–2198, 2017.
[27] A. Tiurlikova, N. Stepanov, and K. Mikhaylov, "Method of assigning spreading factor to improve the scalability of the lorawan wide area network," in *2018 10th International Congress on Ultra Modern Telecommunications and Control Systems and Workshops (ICUMT)*. IEEE, 2018, pp. 1–4.
[28] O. Georgiou and U. Raza, "Low power wide area network analysis: Can lora scale?" *IEEE Wireless Communications Letters*, vol. 6, no. 2, pp. 162–165, 2017.
[29] J. Haxhibeqiri, I. Moerman, and J. Hoebeke, "Low overhead scheduling of LoRa transmissions for improved scalability," *IEEE Internet of Things Journal*, vol. 6, no. 2, pp. 3097–3109, 2018.
[30] M. Rizzi, P. Ferrari, A. Flammini, E. Sisinni, and M. Gidlund, "Using lora for industrial wireless networks," in *2017 IEEE 13th International Workshop on Factory Communication Systems (WFCS)*. IEEE, 2017, pp. 1–4.
[31] L. Tessaro, C. Raffaldi, M. Rossi, and D. Brunelli, "Lightweight synchronization algorithm with self-calibration for Industrial LoRa Sensor Networks," in *2018 Workshop on Metrology for Industry 4.0 and IoT*. IEEE, 2018, pp. 259–263.
[32] R. Piyare, A. L. Murphy, M. Magno, and L. Benini, "On-demand TDMA for energy efficient data collection with LoRa and wake-up receiver," in *2018 14th International Conference on Wireless and Mobile Computing, Networking and Communications (WiMob)*. IEEE, 2018, pp. 1–4.
[33] T. Janssen, N. BniLam, M. Aernouts, R. Berkvens, and M. Weyn, "LoRa 2.4 GHz Communication Link and Range," *Sensors*, vol. 20, no. 16, p. 4366, 2020.
[34] F. R. Andersen, K. D. Ballal, M. N. Petersen, and S. Ruepp, "Ranging Capabilities of LoRa 2.4 GHz," in *2020 IEEE 6th World Forum on Internet of Things (WF-IoT)*. IEEE, 2020, pp. 1–5.
[35] L. Polak and J. Milos, "LTE and LoRa in the 2.4 GHz Band: Adjacent Channel Interference Issues," in *2020 30th International Conference Radioelektronika (RADIOELEKTRONIKA)*. IEEE, 2020, pp. 1–4.
[36] J. Shi, X. Chen, and M. Sha, "Enabling Direct Messaging from LoRa to ZigBee in the 2.4 GHz Band for Industrial Wireless Networks," in *2019 IEEE International Conference on Industrial Internet (ICII)*. IEEE, 2019, pp. 180–189.
[37] S. Escolar, A. Caruso, S. Chessa, X. Del Toro, F. J. Villanueva, and J. C. López, "Statistical Energy Neutrality in IoT Hybrid Energy-Harvesting Networks," in *2018 IEEE Symposium on Computers and Communications (ISCC)*. IEEE, 2018, pp. 00 444–00 449.
[38] L. Hou, S. Tan, Z. Zhang, and N. W. Bergmann, "Thermal energy harvesting WSNs node for temperature monitoring in IIoT," *IEEE Access*, vol. 6, pp. 35 243–35 249, 2018.
[39] I.-J. Hwang, D. Kwon, D.-J. Lee, J.-W. Yu, and W.-S. Lee, "EM/light hybrid energy harvesting with directional dipole antenna for IoT sensor," in *2015 IEEE International Symposium on Antennas and Propagation & USNC/URSI National Radio Science Meeting*. IEEE, 2015, pp. 1292–1293.
[40] H. H. R. Sherazi, M. A. Imran, G. Boggia, and L. A. Grieco, "Energy harvesting in lorawan: A cost analysis for the industry 4.0," *IEEE Communications Letters*, vol. 22, no. 11, pp. 2358–2361, 2018.
[41] J. C. Rodriguez, V. Nico, and J. Punch, "Powering Wireless Sensor Nodes for Industrial IoT Applications using Vibration Energy Harvesting," in *2019 IEEE 5th World Forum on Internet of Things (WF-IoT)*. IEEE, 2019, pp. 392–397.
[42] M. Molefi, E. D. Markus, and A. Abu-Mahfouz, "Wireless Power Transfer for LoRa Low-Power wide-area Networks (LPWANs)," in *2019 Southern African Universities Power Engineering Conference/Robotics and Mechatronics/Pattern Recognition Association of South Africa (SAUPEC/RobMech/PRASA)*. IEEE, 2019, pp. 105–110.
[43] S. Corporation, "SX1280/1281 Data Sheet DS.SX1280-1.W.APP," https://semtech.my.salesforce.com/sfc/p/#E0000000JelG/a/2R000000HoCW/8EVYKPLcthcKCB_cKzApAc6Xf6tAHtn9.UKcOh7SNmg, 2018, accessed: 2021-11-02.
[44] M. Del Prete, A. Costanzo, A. Georgiadis, A. Collado, D. Masotti, and Z. Popović, "A 2.45-GHz energy-autonomous wireless power relay node," *IEEE Transactions on Microwave Theory and Techniques*, vol. 63, no. 12, pp. 4511–4520, 2015.
[45] M. Chiani and A. Elzanaty, "On the LoRa modulation for IoT: Waveform properties and spectral analysis," *IEEE Internet of Things Journal*, vol. 6, no. 5, pp. 8463–8470, 2019.
[46] S. NV, "STM32L47xxx Advanced Arm-based 32-bit MCU," https://www.st.com/resource/en/reference_manual/dm00083560-stm32l47xxx-stm32l48xxx-stm32l49xxx-and-stm32l4axxx-advanced-armbased-32bit-mcus-stmicroelectronics.pdf, 2020, accessed: 2021-11-02.
[47] ——, "MEMS digital output motion sensor: high-performance ultra-low-power 3-axis accelerometer for industrial applications," https://www.st.com/resource/en/datasheet/iis2dlpc.pdf, 2020, accessed: 2021-11-02.
[48] A. Corporation, "AB18X5 Real-Time Clock," https://abracon.com/Precisiontiming/AB18X5-RTC.pdf, 2020, accessed: 2021-11-02.

Giampaolo Cuozzo received the B.Sc degree with honors in electronics and telecommunications engineering and the M.Sc degree with honors in telecommunications engineering from the University of Bologna, Bologna, Italy, in 2017 and 2019, respectively. He is currently pursuing the Ph.D. in electronics, telecommunications, and information technologies engineering (ETIT) at the University of Bologna.

His research activity is focused on full-stack design of THz systems for Industrial Internet of Things applications and optimizations of 5G-NR networks for URLLC. He is also involved in experimental activities that exploit current wireless technologies, like LoRa, Zigbee and NB-IoT.

Chiara Buratti received the M.Sc. degree in telecommunications engineering from the University of Bologna, Bologna, Italy. She is an Assistant Professor with the University of Bologna. Since 2006, when she started her Ph.D., she has been involved in the research related to wireless networks for the Internet of Things, with particular reference to MAC and routing protocol design. She is currently a Principal Investigator of the COST Innovators' Grant IG15104, IMMUNet. She has been Main proponent of the Cost Action CA20120, INTERACT, and Co-Chair of the EWG on IoT of the Cost Action IRACON, the Dissemination Manager for the FP7 WiserBAN Project, and responsible of the EuWIn@Bologna laboratory, created within the FP7 NoE Newcom#. She has coauthored more than 90 research papers.

Roberto Verdone received the master's degree in electronics engineering and the Ph.D. degree from the University of Bologna. Since 2001, he has been a Full Professor in telecommunications with the University of Bologna. He teaches courses on mobile radio networks, the Internet of Things, vehicular communications, and on project management and soft skills. In 2001, he founded a research group (Radio Networks) working on RRM for mobile systems, MAC, routing and topology aspects of wireless sensor networks, architectures, and technologies for the IoT. Since 2020, he has been the Director of the National Laboratory WiLab, Italy, founded by the National Inter-University Consortium for Telecommunications (CNIT). In particular, he is active in the field of the integration of the IoT with 5G networks. He is a part of the Networld2020 Expert Group. In such role, in 2015, he edited a White Paper on Experimental Facilities for 5G in Europe, contributed by about 50 experts from major European stakeholders. He has published about 200 research papers, on IEEE journals/conferences. In the past 15 years, he has been involved/has coordinated more than ten European research projects, including four Networks of Excellence, and many industrial projects (with Telecom Italia, Microsoft, CEA-LETI, and others). During the last decade, he was the General Chairman of the COST Action 2100 on mobile radio communications and co-chaired the follow-up Actions IC1004 and IRACON. In September 2018, he hosted the IEEE PIMRC, Bologna, acting as the General Chairperson. In 2016, he co-founded an innovative start-up (IDESIO).